Investigations on Cold Forming Effect of Cold-drawing Duplex Stainless Steel Tube

Jiachang Wang[a], Baofeng Zheng[a], Ganping Shu[a], Qinglin Jiang[b]

School of Civil Engineering, Southeast University, Nanjing, China[(a)]
Jiangsu Dongge Stainless Steel Ware Co., Ltd, Jiangsu, Dongtai, China[(b)]

Abstract

Cold-drawing is currently an important way of forming stainless steel tubes. Compared to cold-rolling, it is more suitable for producing thick-walled tubes with large dimensions. During the cold-drawing process, huge plastic deformation is embedded in the tube, which makes difference on material properties and residual stresses. This paper experimentally measured residual stresses and material properties distributions in six types of cold-drawing tubes, including three square tubes and three circular tubes. All of tubes were made of duplex stainless steel S22053. For circular tubes, the residual stresses were comparatively low due to the annealing treatment. And material properties were similar to those of the virgin sheet. For square tubes, the longitudinal and transverse bending residual stresses were considerable since annealing treatment was not performed at last step of cold-drawing. And material strength were highly enhanced. Base on the residual stresses test data, residual stresses distribution models were proposed for circular tubes and square tubes, respectively. Based on the equivalent strain theory, strength enhancement model were developed. All the material property parameters of the cold drawn tubes were predicted in the strength enhancement model. Therefore, the full range of stress-strain curve can be obtained. Comparisons of the predictions and the test data show that the proposed models were in good accuracy.

Keywords

Cold-drawing Duplex stainless steel tubes Test Residual stresses Strength enhancement

1 Introduction

Duplex stainless steel combines many of the beneficial properties of ferritic and austenitic steels. Due to the high content of chromium and nitrogen, and often also molybdenum, these steels offer good resistance to localised and uniform corrosion. The duplex microstructure contributes to the high strength and high resistance to stress corrosion cracking. Duplex steels have good weldability [1].

Currently, cold forming methods of stainless steel tubes include cold-rolling and cold-drawing. This paper focused on the cold forming effect of cold-drawing stainless steel tubes. Compared to cold-rolling, cold-drawing is more suitable for producing thick-walled tubes with large dimensions, which are widely employed as bearing members in structures or pressure pipeline.

The cold-drawing circular tubes begin with circular tube blanks which are often small-sized and thick-walled, so the diameter of the blanks needs to be expanded. Then the blanks have to undergo multiple cold-drawing process to adjust the size to obtain the final tubes. If further cold-drawing process requested, annealing shall be conducted to soft the material. The cold-drawing square tubes are based on circular tubes with proper perimeter and thickness. A pair of round-to-square dies are used to reshape the tubes. To maintain the flattening of the surface, annealing would not be performed for square tubes. A brief sketch of round-to-square cold-drawing process is shown in Fig. 1.

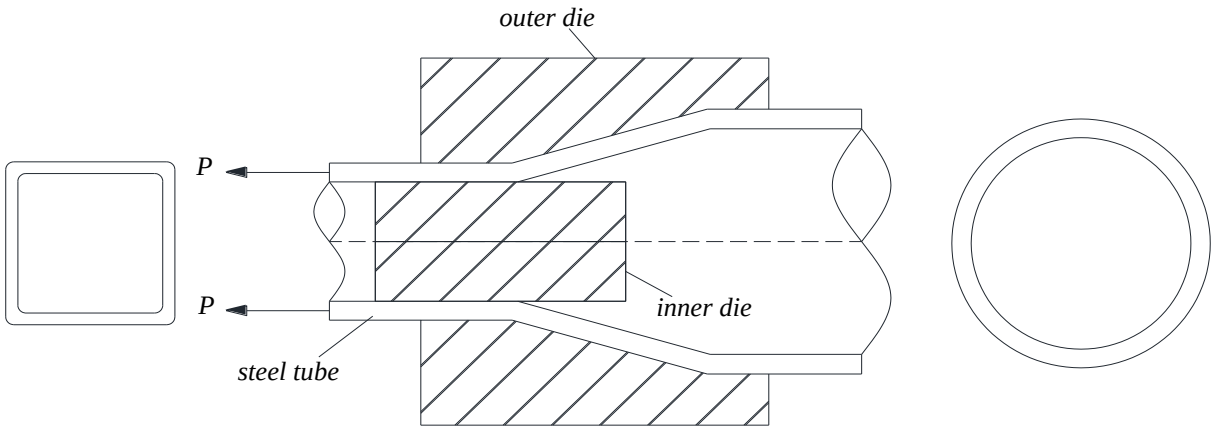

Fig. 1 The brief sketch of round-to-square cold-drawing process

The cold forming effect of cold rolled stainless steel has been extensively investigated [2-9]. The residual stresses distribution models [3],[5] and the strength enhancement models [6],[7],[9] were proposed. However, few researches were

conducted on the cold drawing stainless steel tubes. Ref. [10] carried out material tensile tests on cold drawing austenitic stainless steel square tubes, and indicated the material yield stress was highly enhanced.

The object of this paper is to develop residual stresses distribution models and strength enhancement models of cold-drawing duplex stainless steel square tubes and circular tubes. Firstly, a series of tests were carried out to obtain the residual stresses and material properties of the cold-drawing tubes. And then statistical method and equivalent strain theory were applied to build residual stresses distribution models and strength enhancement models, respectively.

2 Experimental Investigations

The tests of this paper included residual stresses tests and material properties tests on cold-drawing duplex stainless steel tubes of grade S22053(022Cr23Ni5Mo3N) made in China. The test specimens consisted of three kinds of square tubes and three kinds of circular tubes, namely square tube 60×3mm, square tube 80×3mm, square tube 120×3mm, circular tube 76×3mm, circular tube 102×3mm and circular tube 120×3mm, respectively.

2.1 Residual stress tests

Residual stresses in cold-formed sections are generally expected to have substantial bending part and comparatively low membrane part. Bending residual stresses includes longitudinal bending residual stresses and transverse bending residual stresses. This paper focused on bending residual stresses and ignored membrane residual stresses.

2.1.1 Longitudinal bending residual stresses

Sectioning method is a common method for the measurement of residual stresses in built-up stainless steel sections [11-12]. The main procedures involve drilling holes sequentially cutting out strips of the specimen and measuring the change in the distance between the holes using Whittemore gauge. This method is suitable for members in which the longitudinal membrane stresses are dominant [13]. The method is improper for cold-drawing stainless steel tubes since the transverse and the longitudinal bending residual stresses are the major stresses due to the extensive plastic deformation in both the transverse and longitudinal directions [14]. In this paper, the traditional sectioning method was modified by measuring rise of the strips during cutting process. Cutting operation was performed using an automatic electric spark wire cutting machine with minimal heat input into strips. The cutting duration for one pair of strips lasted for approximately 30 minutes.

Considering the size of the cross section and the difficulty of sectioning, the cutting scheme was determined as follows. For square tube 60×3 mm, five strips with width of 8mm were cut out from each flat region and 24 strips were totally obtained including four corner strips. For square tube 80×3mm, seven strips with width of 9 mm were cut out from each flat region and 32 strips were totally obtained including four corner strips. For square tube 120×3 mm, nine strips with width of 11 mm were cut out from each flat region and 40 strips were totally obtained including four corner strips. For circular tubes, 12 strips with width of 8-12 mm, evenly distributed along the cross section, were extracted for each type of tubes. The distribution and numbers of the strips (measuring points) along the cross section are shown in Fig.2.

To minimise the interaction among the strips when cutting one of them, five specimens were used for square tubes and two specimens were used for circular tubes. Typical strip arrangements for square tube 80×3 mm and circular tube 76×3 mm are shown in Fig.3 and Fig.4, respectively. The length of the specimen was 150mm and 2 times the height of the section. The 150 mm range was the cutting area of the strip and 1 times the height of the section was set on both sides to ensure that the residual stresses field in the specimen was consistent with those in the original tubes.

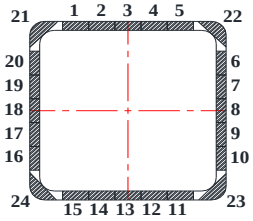

(a) Square tube 60×3mm

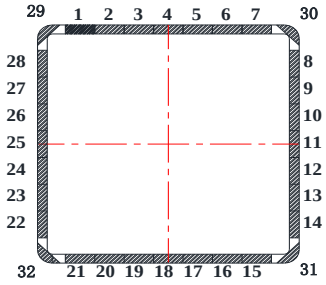

(b) Square tube

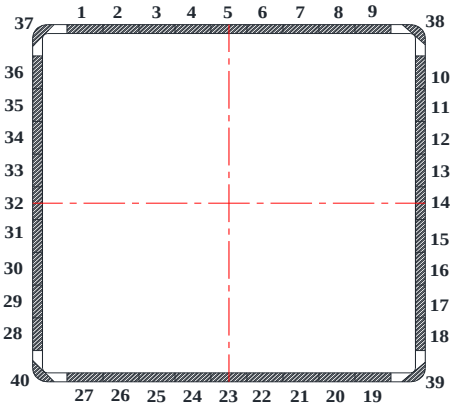

(c) Square tube 120×3mm

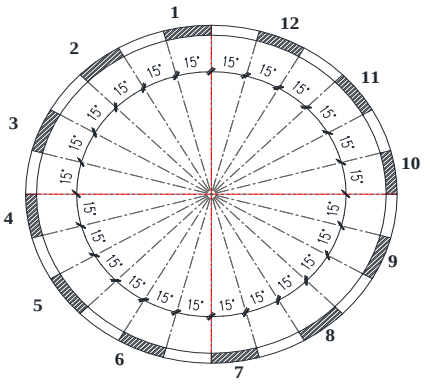

(d) Circular tube 60×3mm

Fig. 2 The distribution and numbers of the measuring points along the cross section

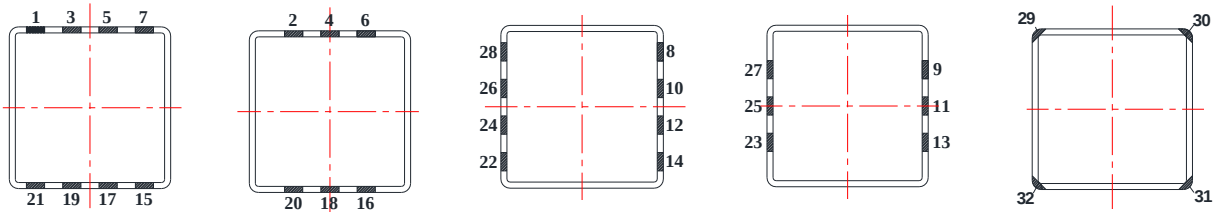

(a) Specimen 1 (b) Specimen 2 (c) Specimen 3 (d) Specimen 4 (e) Specimen 5

Fig. 3 The measuring points of five specimens on the section of square tube 80×3mm

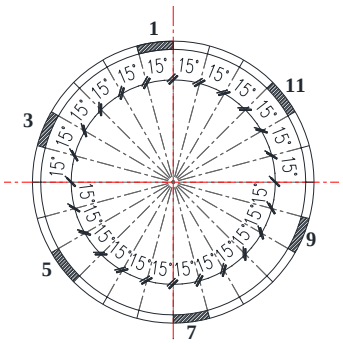

(a) Specimen 1

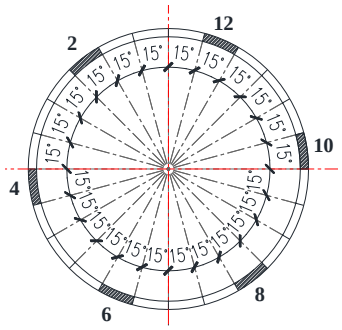

(b) Specimen 2

Fig. 4 The measuring points of two specimens on the section of circular tube 76×3mm

Due to the release of the longitudinal bending residual stresses, the strips appeared obvious bending deformation. All the strips were bent outward after cutting out, indicating that the inner surface of the tube was in compression and the outer surface was in tension. In this paper, the longitudinal bending residual stresses in the strips were predicted by measuring the rise of the strips. It was supposed that the longitudinal bending residual stresses distributed evenly along the length of the strips and the residual stresses released elastically. It meant the strips worked like a simply supported beam subjected a uniform moment. Therefore, provided the rise of the strip was known, the longitudinal bending moment could be calculated according to structural mechanics methods. Then the longitudinal bending residual stresses were assumed to be rectangular in the thickness direction. The longitudinal bending residual stresses in the outer surface of the strip was

calculated according to stress equilibrium. The calculation model and the formula of the longitudinal bending residual stresses are illustrated in Fig.5 and Eq. (1), respectively.

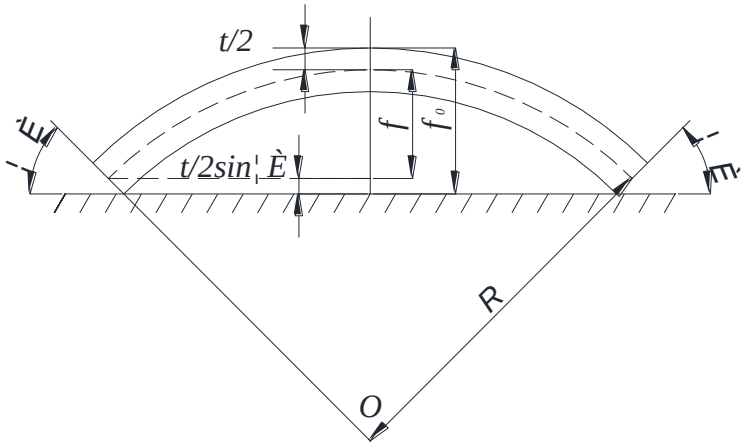

Fig. 5 The calculation model of the longitudinal bending residual stresses

$$\begin{cases} f_0 = f + \dfrac{t}{2} + \dfrac{t}{2}\sin\theta \\ f = R(1-\sin\theta) \\ L = R(\pi - 2\theta) \\ \sigma_r = \dfrac{2}{3}\dfrac{t}{2R}E \end{cases} \tag{1}$$

The nomenclature of f_0、f、t、θ、R is defined in Fig.5. L represented the axis line length of the strip which was 150mm in the test. σ_r was the longitudinal bending residual stresses in the outer surface of the strip and E was Young's modules. The equation should be calculated by iterative numerical methods.

Table 1 The rise and residual stresses of the strips from square tube 60×3mm

Measuring points	Rise /m	Thickness /mm	σ_r /MPa	Measuring points	Rise /mm	Thickness /mm	σ_r /MPa
1	9.02	3.02	446.48	13	7.32	3.02	308.86
2	7.16	2.98	296.19	14	8.34	2.91	381.42
3	5.14	2.88	154.05	15	9.60	3.15	478.23
4	5.42	3.01	171.74	16	10.44	3.15	562.23
5	7.24	3.03	303.33	17	8.00	2.96	355.89
6	9.22	3.02	458.49	18	6.62	3.03	258.33
7	5.96	2.90	210.52	19	6.68	3.00	262.23
8	5.62	2.86	187.14	20	8.88	3.11	416.87
9	6.54	2.95	251.52	21	4.76	3.89	78.84
10	7.24	3.04	303.60	22	5.1	3.97	104.20
11	8.52	3.05	400.99	23	3.74	3.77	14.81
12	7.72	2.94	334.76	24	4.82	4.15	65.77

Table 2 The rise and residual stresses of the strips from circular tube 76×3mm

Measuring points	Rise /mm	Thickness/mm	σ_r /MPa
1	3.78	3.08	50.92
2	3.42	3.02	30.63
3	3.68	3.05	45.68
4	3.20	2.93	22.42
5	3.34	3.03	25.53
6	3.06	2.95	14.95
7	3.12	2.95	17.63
8	3.14	2.96	18.18
9	3.04	2.90	15.88
10	3.78	3.01	54.54
11	3.36	2.94	30.92
12	3.64	3.04	43.54

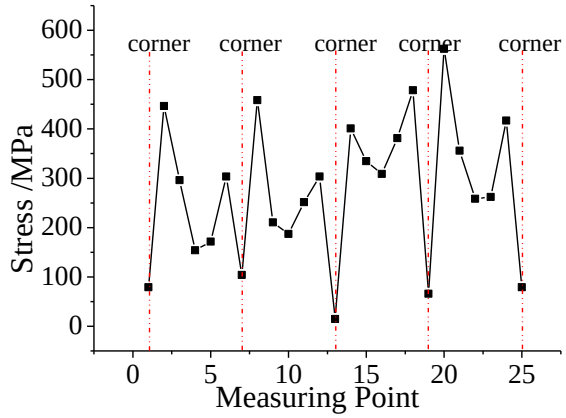

(a) Square tube 60×3mm

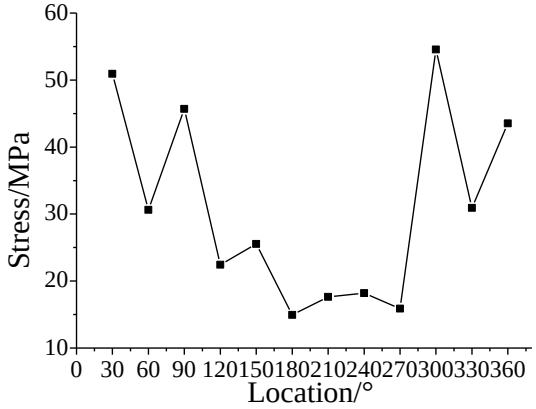

(b) Circular tube 76×3mm

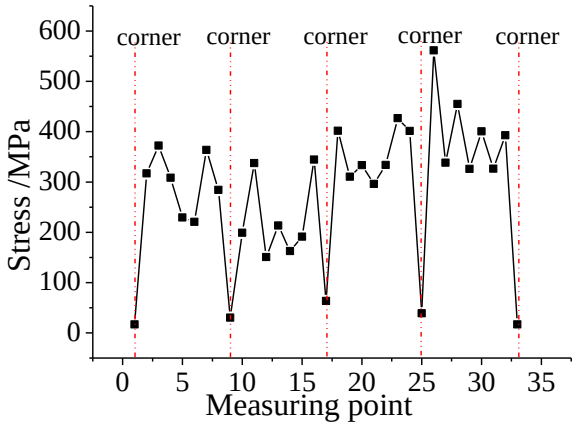

(c) Square tube 80×3mm

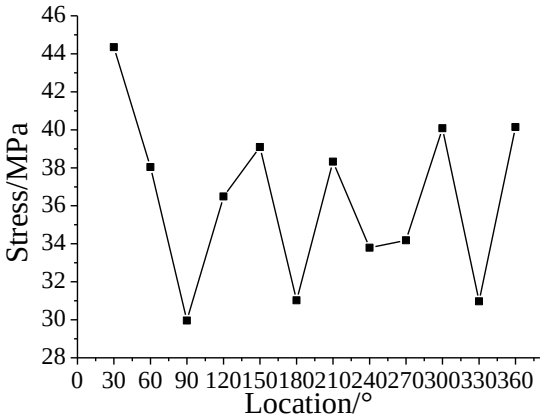

(d) Circular tube 102×3mm

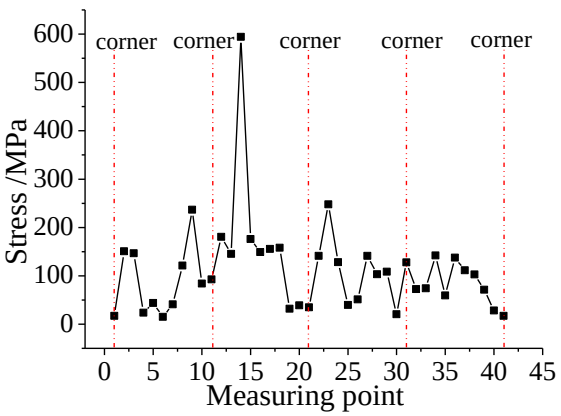

(e) Square tube 120×3mm

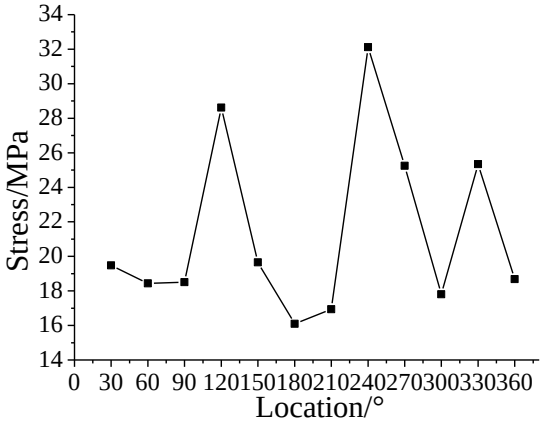

(f) Circular tube 120×3mm

Fig. 6 The longitudinal bending residual stresses at each measuring point

Tables 1 and Table 2 present the rise of the strips and the calculated longitudinal bending residual stresses of square tube 60×3mm and circular tube 76×3mm, respectively. Fig.6 shows the distribution of longitudinal bending residual stresses at different measuring points. The abscissa is the measuring points and the ordinate is the longitudinal bending residual stresses.

The test results demonstrates: (1) The longitudinal bending residual stresses were positive in Table 1 and Table 2 indicating that the outer surface of the section was in tension. (2) The longitudinal bending residual stresses were lower in the centre of the flat face, and grew dramatically from the centre to the intersection point of the flat face and the corner followed by a sharp drop appeared in the corner. (3) The longitudinal bending residual stresses of circular tubes were much lower with the magnitude less than 50MPa.

2.1.2 Transverse bending residual stresses

Splitting method is a common method for the measurement of transverse residual stresses in stainless steel sections. The main procedures involve splitting the specimens along the length direction and measuring the demission of the notch caused by splitting. The splitting position of square tubes was on the centre of the flat face while that of circular tubes was chosen at any position due to symmetry. One specimen was cut out from each kind of tubes, a total of six specimens. The length of the specimen was the height of the section. Cutting operation was performed using an automatic electric spark wire cutting machine with minimal heat input into strips.

Due to the release of the transverse bending residual stresses, the specimens appeared a large notch. The specimens were bent outward after splitting, indicating that the inner surface of the tube was in compression and the outer surface was in tension. In this paper, the transverse bending residual stresses in the section were predicted by measuring the demission of the notch. It was supposed that the transverse bending residual stresses distributed evenly along the section and the residual stresses released elastically. It meant the specimens worked like a simply supported curved beam subjected a uniform moment. Therefore, provided the demission of the notch was known, the transverse bending moment could be calculated according to structural mechanics methods. Then the transverse bending residual stresses were assumed to be rectangular in the thickness direction. The transverse bending residual stresses in the outer surface of the specimen was calculated according to stress equilibrium. The calculation model and the formula of the transverse bending residual stresses are illustrated in Fig.7 and Eq. (2), respectively.

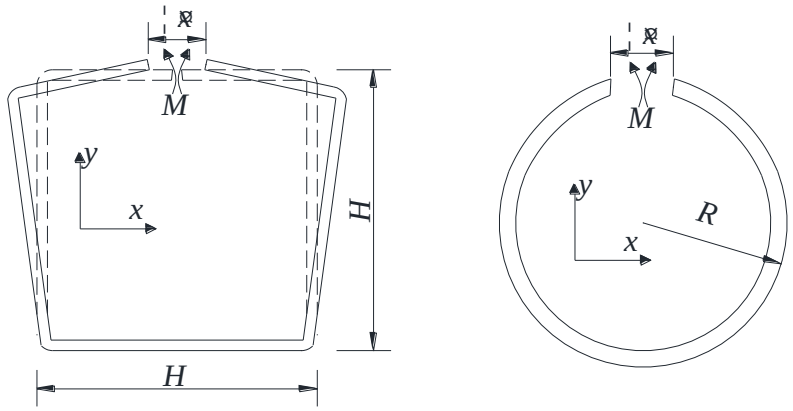

Fig. 7 The calculation diagram of transverse bending residual stresses

$$\begin{cases} \sigma_s = \dfrac{Et\Delta_x}{6H^2} \\ \sigma_c = \dfrac{Et\Delta_x}{6\pi R^2} \end{cases} \quad (2)$$

σ_s was the transverse bending residual stresses in the outer surface of square tubes, σ_c was the transverse bending residual stress in the outer surface of circular tubes, Δ_x was the dimension of the notch, H was the height of square tubes and R was the radius of circular tubes. The Young's modulus E was approximately 200000MPa and the thickness t was 3mm.

Table 3 The transverse bending residual stresses of square tubes

The type of section	H/mm	Δ_x/mm	σ_s/MPa
Square tube 60×3mm	60	9.5	263.89
Square tube 80×3mm	80	13	203.13
Square tube 120×3mm	120	14.1	97.92

Table 4 The transverse bending residual stresses of circular tubes

The type of section	R/mm	Δ_x/mm	σ_c/MPa
Circular tube 76×3mm	38	8.3	182.96
Circular tube 102×3mm	51	11.5	140.74
Circular tube 120×3mm	60	12.8	113.18

Tables 3 and Table 4 present the dimension of the notch and the calculated transverse bending residual stresses of square tubes and circular tubes, respectively. The test results demonstrates: (1) The transverse bending residual stresses were positive in Table 3 and Table 4 indicating that the outer surface of the section was in tension. (2) The transverse bending residual stresses of square tubes and circular tubes were related to the demission of the cross section. The larger the demission of the cross section was, the smaller the residual stresses were.

2.2 Strength enhancement tests

The test coupons included coupons of the virgin sheet before forming and coupons of the tubes after forming. Two standard tensile coupons were made of virgin sheet in 10mm thick after annealing. The standard tensile coupons were fabricated in accordance with the regulations in GB/T 228.1-2010 [15]. The strips cut in the longitudinal bending residual stress tests were used as test coupons of the tubes after forming. For the flat regions of square tubes, the strips on one of the flat regions were tested. For example, the strips of No.1,2,3,4,5 of square tube 60×3mm (in Fig.2) were selected as test coupons Therefore, square tube 60×3mm , square tube 80×3mm and square tube 120×3mm has five, seven and nine coupons. For the corner regions of square tubes, two strips of each tubes were tested. For circular tubes, half of the strips were tested. For example, the strips of specimen 1 of circular tube 76×3mm (in Fig.4) were selected as test coupons.

2.2.1 Material tensile tests

For the flat regions, material tensile tests were performed in a 300 kN SANS universal testing machine in accordance with the Chinese standard GB/T 228.1-2010 [15]. The gauge length of the coupons was 50mm and the load rate was about 0.5 mm/min before the strain reached 0.02 and 10mm/min afterwards. Prior to testing, a pair of strain gauges (BX120-3AA) were attached on each face of the coupon to obtain the strain-stress curve. The strain gauges would peeled off when the strain exceeds 0.02, so the extensometer was used to obtain the full range strains curve. Every square tube was tested with 2 corner coupons. The loading device, the loading rate and the measurement plan in the test were same as those of tensile test of the flat regions.

During the test, some strain gauges peeled off early and the test data were abnormal. After summarizing the valid data, the material properties according to the material model in Ref. [16] for stainless steel tubes are shown in Table 5 and Table 6. In Table 5, 'M' 'S' 'C' in the name of coupons represented virgin sheet, square tubes and circular tubes. The number immediately followed by the letter was the cross section dimension of the coupons. The last number in the name represented the number of the corresponding measuring point in the residual stresses tests. In Table 6, 'CR' in the name of coupons represented the corner coupons. In these tables, E_0 was the material Young's modulus, $\sigma_{0.2}$ was the material 0.2% proof stress, n was a strain hardening exponent, $\sigma_{1.0}$ was the material 1.0% proof stress, $n_{0.2,1.0}$ was a strain hardening exponent representing a curve that passed through 0.2 and 1.0, σ_u was the ultimate tensile stress, δ was the percentage elongation after fracture, ε_u was the ultimate tensile strain.

Table 5 Material tensile test results of the flat regions

Coupons	E_0 /MPa	$\sigma_{0.2}$ /MPa	$\sigma_{1.0}$ /MPa	σ_u /MPa	ε_u	n	$n_{0.2,1.0}$	δ/ %
M-1	190730	551.81	612.78	769.58	0.2300	3.51	3.64	44
M-2	193470	560.81	617.97	773.18	0.2100	4.28	3.26	44
Average	**192100**	**556.31**	**615.38**	**771.38**	**0.2200**	**3.90**		**44**
C76-1	206167	548.57	628.25	772.58	0.2187	5.23	3.60	
C76-3	206071	519.73	622.85	768.73	0.2866	3.69	4.08	36
C76-5	201251	553.16	609.10	760.78	0.2661	7.75	3.27	35
C76-7	206451	513.11	591.56	757.06	0.2834	6.03	2.96	36
C76-11	204469	558.86	619.07	779.63		7.66	2.59	
Average	**204882**	**538.69**	**614.17**	**767.76**	**0.2637**	**6.07**	**3.30**	**36**
C102-1	197048	508.15	594.21	738.81	0.2352	4.83	3.01	33
C102-3	199181	500.45	600.84	769.92		4.03	3.16	
C102-5	194498	498.40	595.08	756.54		4.29	3.13	
C102-7	197254	502.89	581.63	716.58	0.2713	5.95	3.03	40
C102-11	191362	465.36	542.75	678.51	0.2667	5.03	3.02	38
Average	**195869**	**495.05**	**582.90**	**732.07**	**0.2577**	**4.83**	**3.07**	**37**
C120-1	225629	586.95	644.39	789.47	0.2667	7.11	2.79	38
C120-3	226514	567.23	634.40	789.53	0.3035	6.85	2.51	42
C120-5	231491	594.62	656.10	805.42	0.2615	6.65	2.80	36
C120-7	239766	615.00	681.34	834.90	0.2771	5.88	2.90	38
C120-9	274618	641.75	705.21	872.03	0.2626	6.93	2.86	36
C120-11	246133	636.24	702.05	853.34	0.2423	5.99	2.75	
Average	**240692**	**606.96**	**670.58**	**824.11**	**0.2689**	**6.57**	**2.77**	**38**
S60-1	192718	824.94	961.98	974.14	0.0212	5.10	3.45	13
S60-2	217453	790.35	923.37	931.92	0.0198	3.78	3.97	
S60-3	205796	802.03	917.63	921.33	0.0209	3.57	5.18	16
S60-4	201148	815.64	921.11	923.94	0.0207	3.83	5.86	
S60-5	208911	823.90	972.58	983.75	0.0206	3.97	3.54	
Average	**205205**	**811.37**	**939.33**	**947.02**	**0.0206**	**4.05**	**4.40**	**15**
S80-1	209964	903.12	1029.40	1029.44	0.0147	5.88	5.53	
S80-2	200029	779.80	928.37	937.80	0.0218	5.27	4.44	
S80-3	209881	795.77	943.79	950.64	0.0190	4.30	4.11	
S80-4	208766	806.73	923.56	931.18	0.0206	5.63	4.00	12
S80-6	222111	812.95	959.02	965.48	0.0210	4.91	4.59	
S80-7	214321	867.42	1028.29	1033.83	0.0171	4.40	4.32	
Average	**210845**	**827.63**	**968.74**	**974.73**	**0.0199**	**5.06**	**4.50**	**12**
S120-3	220983	865.69	921.12	921.53	0.0201	3.72	13.29	
S120-5	213141	874.55	903.85	905.13	0.0199	4.53	8.42	
S120-6	217051	848.37	884.04	885.09	0.0169	4.42	6.69	
S120-7	221214	858.29	909.99	912.17	0.0200	5.50	5.35	17
Average	**218097**	**861.72**	**904.75**	**905.98**	**0.0192**	**4.54**	**8.44**	**17**

Table 6 Material tensile test results of the corner regions

Coupons	E_0 /MPa	$\sigma_{0.2}$ /MPa	$\sigma_{1.0}$ /MPa	σ_u /MPa	n	$n_{0.2,1.0}$	δ/%
S60-1-CR	162940	1087.8	1168.50	1174.2	9.97	3.21	8
S60-2-CR	177230	1104.6	1146.50	1147.0	8.52	2.53	10
Average	**170085**	**1096.2**	**1157.50**	**1160.6**	**9.25**	**2.87**	**9**
S80-1-CR	211550	1088.7	1133.10	1134.6	3.10	2.76	10
S80-2-CR	196820	1087.9	1107.90	1109.5	4.37	7.19	8
Average	**204185**	**1088.3**	**1120.50**	**1122.1**	**3.74**	**4.98**	**9**
S120-1-CR	165060	1133.6		1136.4	18.77		10
S120-2-CR	198320	1107.5		1148.7	3.76		9
Average	**181690**	**1120.6**		**1142.5**	**11.30**		**10**

It can be seen from Table 5: (1) The material Young's modulus E_0 of duplex stainless steel S22053 roughly distributed around 200000 MPa for virgin sheets, square tubes and circular tubes. (2) The material properties of circular tubes were similar to those of virgin sheets. For example, the proof stress of virgin sheets were 556.31MPa and the proof stress of circular tube 76×3mm were 538.69MPa. It indicated that strength enhancement of circular tubes was not obvious. (3) Compared with the proof stress of virgin sheets, the proof stress of square tubes was considerably improved, even higher than the ultimate tensile stress. (4) The ultimate tensile strain of square tubes was dramatically decreased to 0.02.

It can be seen from Table 6: (1) The proof stress reached up to 1000 MPa, about two times that of virgin sheets. (2) The proof stress and the ultimate tensile stress were very close, which meant the material of corner regions had no obvious strain hardening properties. (3) The percentages of elongation were less than 10%.

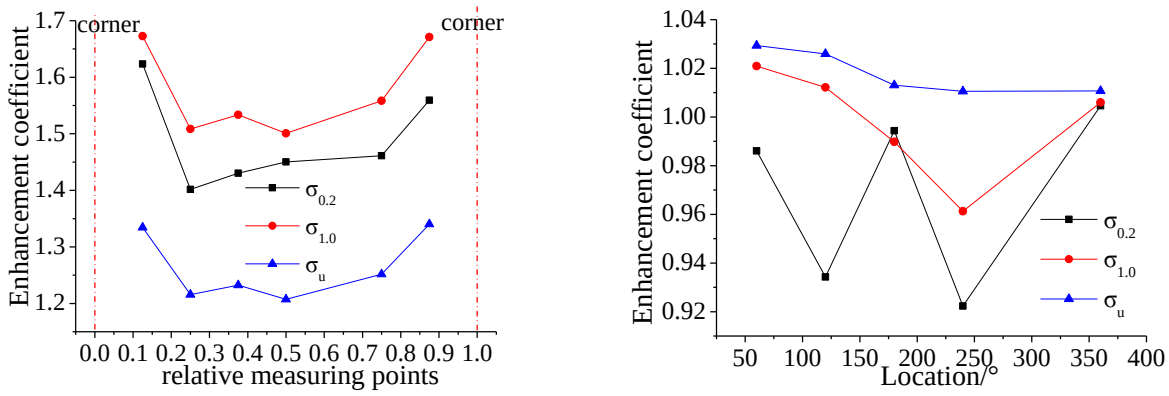

(a) Square tube 80×3mm **(b) Circular tube 76×3mm**

Fig. 8 The distribution of strength enhancement coefficient

In Fig.8, the material properties of the cold-drawing tubes were normalised by those of the virgin sheet. The ratio between $\sigma_{0.2}$, $\sigma_{1.0}$, σ_u of the flat regions to those of the virgin sheet was used as enhancement coefficient. Taking square tube 80×3mm and circular tube 76×3 mm as an example in Fig.8, the black line, red line and blue line indicate the enhancement coefficient of $\sigma_{0.2}$, $\sigma_{1.0}$ and σ_u, respectively.

It can be concluded: (1) The enhancement coefficients of circular tube were close to 1.Therefore, the strength enhancement of circular tubes can be neglected. (2) The ratio of the proof stress of square tubes to that of the virgin sheet was up to 2.0 at the corner and decreases continually to 1.4 at the centre of the flat face. The line for the ultimate stress σ_u lay below the line for the proof strength $\sigma_{0.2}$, which meant the ultimate stress σ_u was not so sensitive to cold working than the proof stress $\sigma_{0.2}$.

3 Residual Stresses Distribution Model

3.1 Longitudinal bending residual stresses distribution model

Based on the test data, the longitudinal bending residual stresses of circular tubes could be neglected. Therefore, this paper only considered the longitudinal bending residual stresses of square tubes. To develop a distribution model, the longitudinal bending residual stresses of square tubes were firstly normalised using the material proof stress ($\sigma_{0.2}$ in Table 5) and the positions of measuring point on the flat face were normalised by the width of the cross section. The results were shown in Fig.9. The residual stresses distribution of square tubes on the flat regions can be divided into two parts: 0.5 times the width of the centre of the flat regions and the other regions. The residual stresses of the centre regions were relatively lower than those of the other regions. The mean residual stresses of the 0.5 times the width of the centre of the flat regions were 0.30 times of the proof stress of square tubes. For the other regions, the value was 0.43 times of the proof stress of square tubes. For the corner regions, the value was 0.05 times of the proof stress of square tubes. The longitudinal residual stresses distribution model of cold-drawing duplex stainless steel square tubes are shown in Fig.10, where $f_{0.2\text{-S}}$ is the proof stress of the flat regions, $f_{0.2\text{-SCR}}$ is the proof stress of the corner regions and H is the width of square tube.

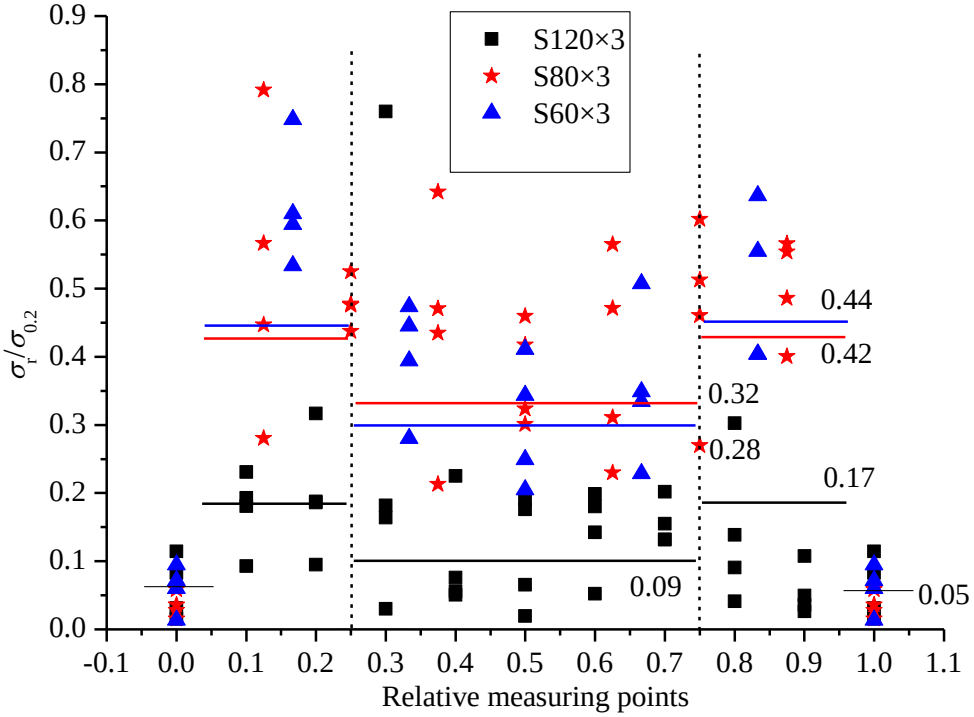

Fig. 9 The longitudinal bending residual stresses normalized by the material proof stress

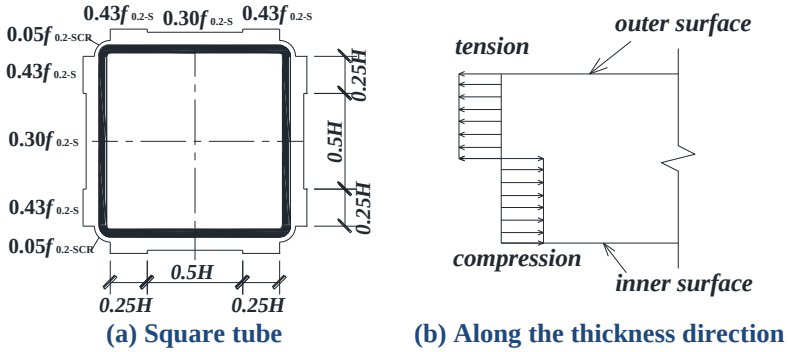

(a) Square tube **(b) Along the thickness direction**

Fig.10 The longitudinal bending residual stresses distribution model

3.2 Transverse bending residual stresses distribution model

The transverse bending residual stresses were assumed to be evenly distributed along the cross section. The ratio of the transverse bending residual stresses to the proof stress is listed in Table 7. With the demission of the cross section increasing, the transverse bending residual stresses decreased. Due to the limited test data, the phenomenon was ignored and the mean value was used to characterise the residual stresses. The mean transverse residual stresses of square tubes

and circular tubes were 0.23 and 0.27 times of the proof stresses, respectively. The transverse bending residual stresses distribution model of cold-drawing duplex stainless steel square tubes and circular tubes are shown in Fig.11.

Table 7 The value of the transverse bending residual stress

The type of section	σ_r/MPa	$\sigma_r/\sigma_{0.2}$
Square tube 60×3mm	263.89	0.33
Square tube 80×3mm	203.13	0.25
Square tube 120×3mm	97.92	0.11
Circular tube 76×3mm	182.96	0.34
Circular tube 102×3mm	140.74	0.28
Circular tube 120×3mm	113.18	0.19

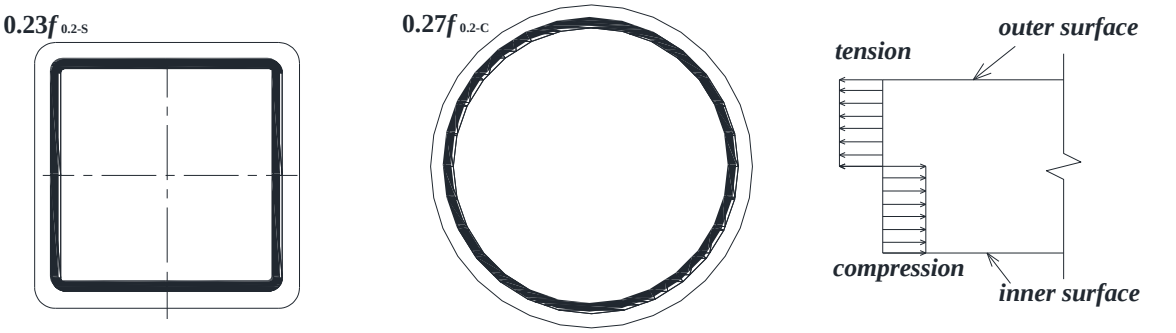

(a) Square tube (b) Circular tube (c) Along the thickness direction

Fig. 11 The transverse bending residual stresses distribution model

4 Theoretical Researches on Cold-drawing Strength Enhancement

4.1 Stress-strain curve of virgin sheet

The material properties of virgin sheet in the test only included the material property parameters, lacking the full-range stress-strain curve. But it can be seen from Table 5 and Fig. 8 (b) that the material property parameters of circular tubes were basically the same as those of virgin sheets. Therefore, the test data of circular tubes were used in this paper instead of virgin sheets to propose the model of full-range stress-strain curve.

Based on the observation of the stress-strain curve, two models were selected to fit the curve. Model 1, proposed in ref.[17], was divided into two segments: 0~$\sigma_{0.2}$ and $\sigma_{0.2}$~σ_u and is shown in Eq. (3). Model 2 was also divided into two segments: 0~$\sigma_{0.2}$ and $\sigma_{0.2}$~σ_u. Ramberg-Osgood model was used on 0~$\sigma_{0.2}$, the exponential model was used on $\sigma_{0.2}$~σ_u and is shown in Eq. (4). All model parameters were able to be obtained by the tensile tests. The parameter m in the second equation of model 1 needed to be obtained by fitting the second stage stress-strain curve acquired by the test, which was difficult in the test data processing. In these equations, E_0 was the material Young's modulus, $\sigma_{0.2}$ was the material 0.2% proof stress, n was a strain hardening exponent, $\sigma_{0.01}$ was the material 0.01% proof stress, σ_u was the ultimate tensile stress, ε_u was the ultimate tensile strain.

Fig.12 shows the test stress-strain curve of C76-1, and the fitted curve of Model 1 and Model 2. The fitting results of the two models agreed well with the test data. There were four independent material property parameters (E_0, $\sigma_{0.2}$, σ_u and ε_u) in Model 2 while six (E_0, $\sigma_{0.2}$, σ_u, ε_u, n and m) in Model 1. Model 2 was simple in expression, which could be easily transformed between stress and strain. In terms of precision and convenience, Model 2 was used to represent the stress-strain curve of virgin sheets.

$$\begin{cases} \varepsilon = \dfrac{\sigma}{E_0} + 0.002(\dfrac{\sigma}{\sigma_{0.2}})^n \quad 0 \le \sigma \le \sigma_{0.2} \\ \varepsilon = \dfrac{\sigma - \sigma_{0.2}}{E_{0.2}} + (\varepsilon_u - \varepsilon_{t0.2} - \dfrac{\sigma_u - \sigma_{0.2}}{E_{0.2}})(\dfrac{\sigma - \sigma_{0.2}}{\sigma_u - \sigma_{0.2}})^m + \varepsilon_{t0.2} \quad \sigma_{0.2} \le \sigma \le \sigma_u \\ n = \dfrac{\ln(20)}{\ln(\sigma_{0.2} / \sigma_{0.01})} \\ E_{0.2} = \dfrac{E_0}{1 + 0.002 n E_0 / \sigma_{0.2}} \end{cases} \tag{3}$$

$$\begin{cases} \varepsilon = \dfrac{\sigma}{E_0} + 0.002(\dfrac{\sigma}{\sigma_{0.2}})^n \quad 0 \le \sigma \le \sigma_{0.2} \\ \varepsilon = (\dfrac{\sigma}{p})^q \quad \sigma_{0.2} \le \sigma \le \sigma_u \\ q = \dfrac{\ln(\varepsilon_u / \varepsilon_{0.2})}{\ln(\sigma_u / \sigma_{0.2})} \quad p = \dfrac{\sigma_{0.2}}{\sqrt[q]{\varepsilon_{0.2}}} \end{cases} \tag{4}$$

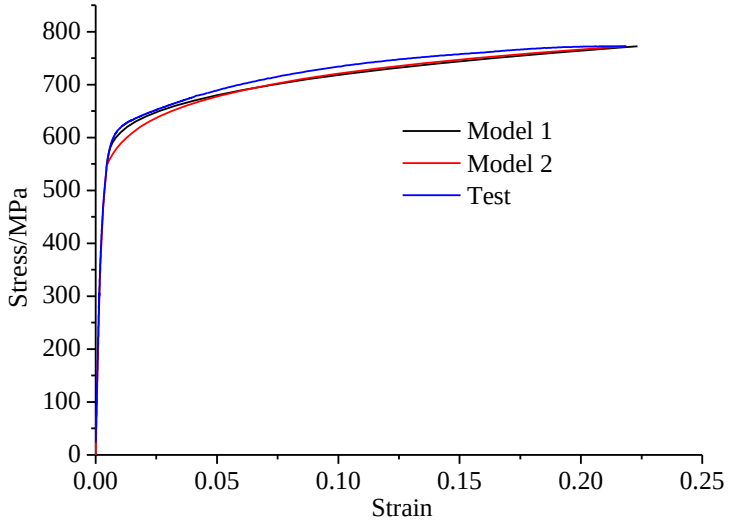

Fig. 12 The simulation of stress-strain curve of base model

4.2 Strength enhancement model

According to the test data, the strength enhancement of circular tubes can be ignored. Therefore, the strength enhancement of square tubes were developed only in this paper. Several prediction models for the proof stress and ultimate stress of cold formed tubes have been proposed [6-9] while part of these models were empirical formulas [6-7]. Rossi [9] developed a model for nominal yield stress by using a power law material model and average plastic strain. The proof stress was obtained by taking the average plastic strain into the power law material model. In this paper, similar idea was employed. Equivalent strain was used instead of the average plastic strain, and was determined for each material parameter.

The maximum plastic strains experienced during cold-drawing were mainly caused by bending, axial tension and circumferential compression. The maximum plastic strains caused by bending can be expressed easily while it was difficult to compute the plastic strains produced by axial tension and circumferential compression. In this paper, by correcting the plastic strain produced by bending, the equivalent strains were obtained.

E_0

Comparison between the initial elastic modulus E0 of the virgin sheet and that of the cold drawn tube shows that E0 was almost the same for these two states. Thus, the initial elastic modulus E0 of the cold drawn tube was approximately equal to that of the virgin sheet.

$\sigma_{0.2,f}$

The prediction model for σ0.2,f is shown in Eq.(5). In this equation, σ0.2,f is the proof stress; p and q are the material parameters of virgin sheets; B, H, t, r0 and R are geometric parameters defined in Fig.13; εeq is equivalent strain for the proof stress.

According to the isotropic hardening assumption, the σ0.2,f was approximately equal to the stress corresponding to the equivalent strain εeq on the stress-strain curve of virgin sheets. The equivalent strain εeq belongs to the second stage of material model. Thus, the stress σ0.2,f can be easily obtained by taking εeq into the second equation of Eq.(4). To increase the accuracy of predictions, an empirical factor (1+εeq) was used.

The equivalent strain εeq for proof stress was determined by fitting the test data, and was 1.2 times of the maximum plastic strain caused by bending plus 0.04. The constant 0.04, also called reducing rate, represented the uniform compression in the transverse direction. The maximum plastic strain caused by bending in the processing of crushing a circular tube to a square tube was t/2rx. Provided that the rx for the calculation point was known, the maximum plastic strain, and the equivalent strain can be solved.

rx varied along the cross section. rx was equal to the radius R of circular tube to be crushed for the centre of the flat face. And rx was equal to the radius of the corner (ro-t/2) for the point on the edge of the flat face. For points between the centre of the flat face and the edge of the flat face, rx was interpolated between R and (ro-t/2) according to the distance away from centre of the flat face. The calculation diagram and the formula of rx for the point with distance x away from centre of the flat face, were illustrated in Fig.13 and last formula in Eq.(5), respectively.

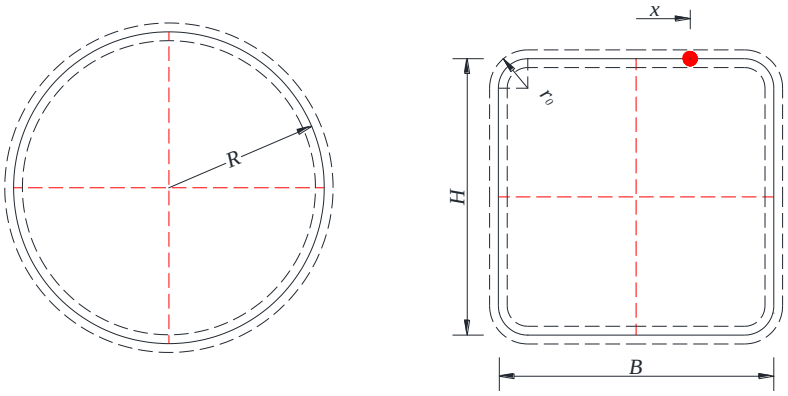

Fig. 13 The calculation diagram of the equivalent strain

$$\begin{cases} \sigma_{0.2,f} = (p\varepsilon_{eq}^{\frac{1}{q}})(1+\varepsilon_{eq}) \\ \varepsilon_{eq} = 1.2\dfrac{t}{2r_x} + 0.04 \\ r_x = \dfrac{2\pi R - 4(1+\dfrac{H}{B})x}{2\pi} \end{cases} \tag{5}$$

$\varepsilon_{u,f}$ and $\sigma_{u,f}$

The prediction model for εu,f and σu,f is shown in Eq.(6). In this equation, εu,f and σu,f are the ultimate strain and ultimate stress, respectively; εu,v and σu,v are the material parameters of virgin sheets. Based on the test data, εu,f was constant for all the coupons from square tubes. Thus, a mean value of 0.02 were used. The true stress at ultimate state σt,u of the virgin material and that of the cold drawing tube were approximately the same. Thus, σu,f can be calculated provided the εu,f was known.

$$\begin{cases} \varepsilon_{u,f} = 0.02 \\ \sigma_{u,f} = \dfrac{\sigma_{t,u}}{1+\varepsilon_{u,f}} = \dfrac{\sigma_{u,v}\left(1+\varepsilon_{u,v}\right)}{1+\varepsilon_{u,f}} \end{cases} \tag{6}$$

n_f

Based on the available test data, the strain hardening exponent in the first stage of the material model is about 0.3 times of the exponent in the second stage. Thus, Eq.(7) was proposed for the strain hardening exponent of the first stage in the material model. In this equation, nf is the working hardening exponent; q is the material parameters of virgin sheets.

$$n_f = 0.3q \tag{7}$$

4.3 Comparisons

All the material properties were calculated by the proposed model (Eq. (5), (6) and (7)).The ratios of test data to predictions of the material properties on the flat regions of square tubes are shown in Table 8.

It can be seen from Table 8: (1) The predictions fitted the test data well. The mean ratios of test data to predictions of σ_u, ε_u, $\sigma_{0.2}$ and n were 1.10, 0.98, 1.05 and 1.01, respectively. (2) The predictions of σ_u and $\sigma_{0.2}$ were conservative, which led to safe design. (3) The strain hardening exponent n was quite scatter because the determination of its value was effected by the test conditions, which existed a certain degree of volatility.

Table 8 The ratios of test data to predictions of the material parameters

Coupons	Test /Prediction					
	x	r_x	σ_u	ε_u	$\sigma_{0.2}$	n
S60×3-1	16	17.01	1.05	1.06	0.97	1.27
S60×3-2	8	27.19	1.08	0.99	0.99	0.80
S60×3-3	0	37.38	1.10	1.04	1.03	0.73
S60×3-4	8	27.19	1.07	1.03	1.02	0.81
S60×3-5	16	17.01	1.06	1.03	0.97	0.99
S80×3-1	27	15.46	1.09	0.73	1.04	1.54
S80×3-2	18	26.92	1.08	1.09	0.97	1.12
S80×3-3	9	38.38	1.14	0.95	1.03	0.87
S80×3-4	0	49.84	1.14	1.03	1.06	1.14
S80×3-6	18	26.92	1.12	1.05	1.01	1.05
S80×3-7	27	15.46	1.09	0.86	1.00	1.15
S120×3-3	22	47.29	1.13	1.01	1.14	0.75
S120×3-5	0	75.30	1.14	1.00	1.19	0.93
S120×3-6	11	61.30	1.10	0.84	1.14	0.90
S120×3-7	22	47.29	1.11	1.00	1.13	1.11
Average			1.10	0.98	1.05	1.01
Variance			0.03	0.09	0.07	0.21
Maximum			1.14	1.09	1.19	1.54
Minimum			1.05	0.73	0.97	0.73

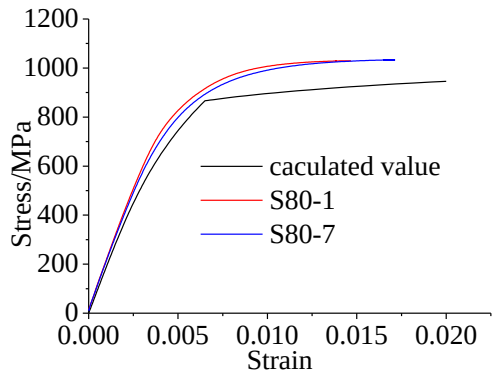

(a) 27mm far away from the centre of the flat face

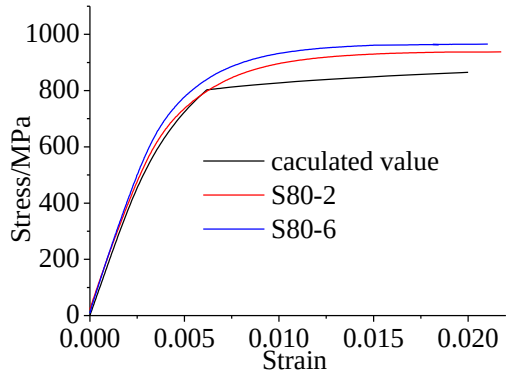

(b) 18mm far away from the centre of the flat face

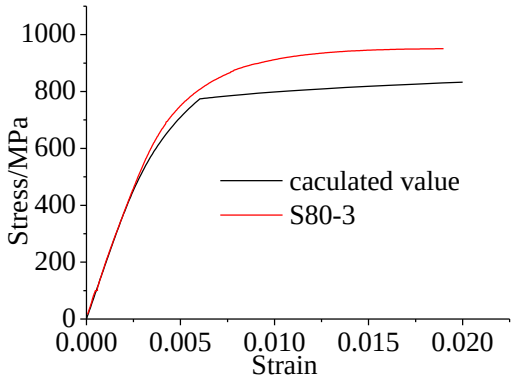

(c) 9mm far away from the centre of the flat face

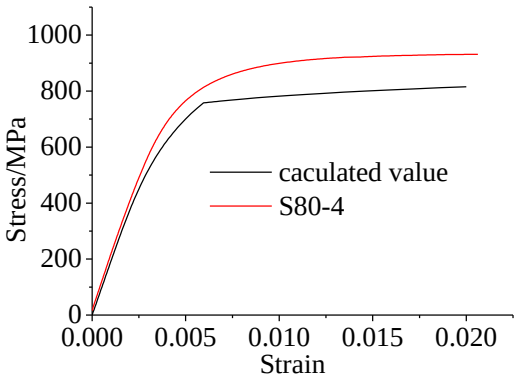

(d) centre of the flat face

Fig. 14 The comparison between the calculated stress-strain curve and the test data of square tube 80×3mm at different distances from the centre of the flat face

Taking the square tube 80×3mm for instance, the comparison between the calculated stress-strain curve and the test data of the cold-drawing material are shown in Fig.14.

It can be seen that: (1) the predicted stress-strain curve was in good agreement with the test data when the stress was lower than $\sigma_{0.2}$ (2) When the stress was higher than $\sigma_{0.2}$, the predicted stress-strain curve lay below the test data but with the same trend.

5 Conclusion

1. The material properties of cold-drawing duplex stainless steel circular tubes were similar to virgin sheets due to annealing after cold-drawing. The longitudinal bending residual stresses and membrane residual stresses were negligible. The transverse bending residual stresses was 0.27 times of the proof stress due to uneven cooling.
2. The longitudinal bending residual stresses on the flat regions of cold-drawing duplex stainless steel square tubes gradually increased from the centre to the edge. The magnitude of longitudinal bending residual stresses on the flat face was up to 0.43 times of the proof stress while those in the corner was extremely small, only 0.05 times of the proof stress. The transverse bending residual stresses uniformly distributed along the cross section and the magnitude was 0.23 times of the proof stress.
3. The strength enhancement of cold-drawing duplex stainless steel square tubes was very considerable. The proof stress of the flat regions was even higher the ultimate tensile stress of virgin sheets while the mean elongation was only 0.02.
4. According to the equivalent strains theory, the strengthening model of the material properties was established and the full range stress-strain curve of the tubes after cold-drawing was obtained. Compared with the test data, the proposed model in this paper had good accuracy.

Acknowledgements

The research work described in this paper is supported by the Priority Academic Program Development of Jiangsu Higher Education Institutions and by the National Science Foundation of China through the projects No. 51378105 and 51578134. The financial support is highly appreciated. Special thanks to the Jiangsu Dongge Stainless steel Ware Co., Ltd. for providing the test specimens.

References

[1] http://www.outokumpu.com/en/Pages/default.aspx

[2] Cruise R.B., Gardner L. Residual stress analysis of structural stainless steel sections. Journal of Constructional Steel Research, 2008, 64: 352-366.

[3] Gardner L., Cruise R.B. Modeling of residual stresses in structural stainless steel sections. Journal of Structural Engineering, 2009, 135(1): 42-53.

[4] Jandera M., Gardner L. and Machacek J. Residual stresses in cold-rolled stainless steel hollow sections. Journal of Constructional Steel Research, 2008, 64: 1255-1263.

[5] Jandera M., Machacek J. Residual stress pattern of stainless steel SHS. Tubular Structures XII, 2010, 265.

[6] Ashraf M., Gardner L., and Nethercot D.A. Strength enhancement of the corner region of stainless steel cross-sections. Journal of Constructional Steel Research, 2005, 61:37-52.

[7] Cruise R.B., Gardner L. Strength enhancements induced during cold forming of stainless steel sections. Journal of Constructional Steel Research 2008; 64(11):1310-6.

[8] Afshan S., Rossi B., Gardner L. Strength enhancements in cold-formed structural sections − part I: material testing. Journal of Constructional Steel Research, 2013, 83:177-88.

[9] Rossi B., Afshan S., Gardner L. Strength enhancements in cold-formed structural sections − Part II: Predictive models. Journal of Constructional Steel Research s, 2013, 83:189-96.

[10] Zheng B.F., Hua X., Shu G.P. Tests of cold-formed and welded stainless steel beam-columns, Journal of Constructional Steel Research 2015, 111: 1‑10.

[11] Lagerqvist O., Olsson A. Residual stresses in welded I-girders made of stainless steel and structural steel. In: Proceedings of the 9th Nordic steel construction conference, 2001, 737-744.

[12] Yuan H.X., Wang Y.Q., Shi Y.J, and Gardner L. Residual stress distributions in welded stainless steel sections. Thin-Walled Structures, 2014, 79: 38-51.

[13] Schajer G.S. Practical residual stress measurement methods. John Wiley & Sons, United Kingdom, 2013.

[14] Tebedge N., Alpten G., and Tall L. Residual-stress measurement by the sectioning method. Experimental Mechanics, 1973, 13(2): 88-96.

[15] GB/T 228.1-2010. Metallic materials-tensile testing-Part 1: Method of test at room temperature. China Standard Press, Beijing, 2010 (in Chinese).

[16] Gardner L. A new approach to stainless steel structural design. PhD Thesis. Structures Section. Department of Civil and Environmental Engineering, Imperial College, London, 2002.

[17] Rasmussen K. J. R. Full-range stress-strain curves for stainless steel alloys. Journal of Constructional Steel Research. 2003, 59:47-61.